Chapter 5

Cross section measurement on Cadmium for the nuclear reactor and astrophysical applications

The multidisciplinary work was conducted in the field of nuclear reactors and astrophysics for the first time. Cadmium has exceptional importance for the development of nuclear reactors and astrophysical applications. The stacked foil activation technique and offline γ ray spectroscopy have been utilized for the present study. We have studied ^{114}Cd(p, γ)^{115m}In, and ^{114}Cd(p, n)^{114m}In reactions for the reactor and astrophysical applications, ^{112}Cd(p, γ)^{113m}In for astrophysical p process, (p, n) and (p, 2n) reaction channels on ^{110}Cd for reactor applications. These reactions were chosen as the scarcity of cross section data found in the previously published data libraries. The astrophysical S factor has been also calculated for ^{114}Cd(p, γ)^{115m}In, ^{114}Cd(p, n)^{114m}In, and ^{112}Cd(p, γ)^{113m}In reactions using their respective cross section data. Statistical nuclear model codes such as ALICE-2014, TALYS-1.95, and EMPIRE-3.2.3 were utilized for statistical model calculations. The simulation of presently evaluated data with previously published data of literature and theoretical calculations was performed. It is concluded that the evaluated data are well matched with the EXFOR data, and the theoretical calculations.

Vibhuti Vashi *et al.*, Phys. Rev. C **105**, 044613 (2022). IF: 3.199
Vibhuti Vashi *et al.*, Proc. of the DAE Symp. on Nucl. Phys. **65** (2021).
Vibhuti Vashi *et al.*, Rad. Phys. and Chem. **208**, 11093 (2023). IF: 2.776

5.1 Introduction

Nuclear data related to the reactions produced using proton beams have many applications in various fields such as nuclear reactors and technology, radioactive waste management, accelerator physics, cyclotrons, production of medical radionuclides, nuclear astrophysics to understand the driving mechanism behind the cause of chemical elements, test the nuclear theories, and many more [1–4]. The experimental study on proton induced nuclear data is also significant to improve the theoretical modeling for fundamental and applied research. We have focused this study on the significance of proton induced reaction data for the application in a nuclear reactor and astrophysics and discussed below.

5.1.1 Importance in Nuclear Reactor Technology

The reactions induced by proton have significant importance for the development and advancement of a new concept of nuclear power generation from nuclear reactors such as compact & high-temperature reactors (CHTR), Accelerator-driven sub-critical systems (ADSs) [5–8], advanced heavy water reactors (AHWRs), and fast reactor [9, 10].

In ADSs, the particles with high energy are bombarded on a heavy radionuclide that produces spallation reactions, which may produce high neutron flux to be used for the transmutation of the isotopes having a long life. In addition to the neutrons, other particles such as protons, α particles, and fission fragments will be produced from the lowest energy to GeV energy range [11, 12]. In recent years, the reactions using these particles became more interesting for finding out suitable materials for the mentioned applications and for withstanding radiation [13].

In fission-based reactors, the fission neutrons slow down in a hydrogenous medium, and a considerable amount of fast recoil protons are generated due to (n, p) interaction, and elastic or inelastic scattering. These protons have enough energy to start the nuclear reactions, such as (p, γ), and (p, n) reactions for light or heavy elements. These reactions can be the origin of different background activities and they are

utilized to generate small radioactive sources which is impossible to generate in the reactor by any means [14].

5.1.2 Importance in Nuclear Astrophysics

Apart from reactor applications, the reactions induced by utilizing protons have prime importance in the field of astrophysical processes. The origin of proton-rich (neutron deficient) stable isotopes with a mass between ^{74}Se and ^{196}Hg, usually named as "p nuclei", that is the topic of discussion [15,16]. Many assumptions are made for the creation of p nuclei. It is believed that proton capture reactions can produce p nuclei in He-accreting sub-Chandrasekhar white dwarfs. The p processes are also presumed to be taking place in a zone of core-collapse supernovae, with the temperature lying between T = 2-3 GK [17]. It is also assumed to be taking place in a singly degenerate type-Ia supernova scenario [18], in the deep O-Ne layers of massive stars like supernova or pre-supernova phases etc. The detailed modeling of p process requires comprehensive knowledge about the stellar environment (temperature, original seed, burning time scale etc.). Nuclear physics plays a key role in modeling. Approximately 20,000 reactions among 2000 nuclei from Ni to Bi (p process network), which requires attention for the measurement of reaction rates [17].

Cadmium is chosen for proton induced study in this work due to its application in the field of nuclear reactors as well as in nuclear astrophysics. It is a naturally occurring silver-white, soft, ductile, and tarnishable metal. It is nearly divalent, and the chemical properties resemble zinc that is found in the earth's crust with a very common impurity of zinc ores [19].

Cadmium is widely used as control rods to control nuclear fission in nuclear reactors (AHWRs, PWR, etc.) due to its high capability to absorb low energy neutrons i.e., thermal neutrons [20,21]. Further, the recoil protons of the reactor may interact with Cd isotopes and can transmute them into different isotopes, and can change the mechanical and other properties of the controlling material [22]. It is also used for radiation shielding purposes in nuclear reactors as well as a different concentration of CdO along with Bismuth Borate glasses is an excellent shielding material to shield

gamma rays in various medical and industrial sectors [23]. Moreover, the nuclear data on ^{nat}Cd are essential to check the consistency of the data obtained with the enriched targets as well as with the evaluated data [24, 25]. Besides application in nuclear reactors, Cadmium is also important for nuclear astrophysics. The proton induced reaction with Cadmium will contribute to the p process reaction network among approximately 20,000 reactions. Cadmium isotopes have some other general industrial applications such as bearing alloys, galvanization, electroplating, manufacturing batteries, and pigments [1, 26, 27].

We have studied ^{114}Cd(p, γ)^{115m}In, ^{114}Cd(p, n)^{114m}In reaction for the nuclear reactors and astrophysical applications for three different proton energies 14.14 $\pm$ 2.03, 10.10 $\pm$ 2.15, and 4.86 $\pm$ 2.40 MeV. Moreover, the reaction cross section was measured for ^{112}Cd(p, γ)^{113m}In reaction at 4.86 $\pm$ 2.40 MeV of proton energy which is relevant to the astrophysical application. The scarcity is observed for the ^{114}Cd(p, γ) reaction in the literature for higher proton energy range [28, 29]. We have studied ^{114}Cd(p, n)^{114m}In reaction utilizing the data obtained from the same experiment, and previously reported data available in the Refs. [30–37]. For ^{112}Cd(p, γ)^{113m}In reaction, only one dataset of A. Psaltis *et al.* (2019) [38] is available in the literature. The astrophysical S factor has been also studied for these reactions. Our motivation for studying these reactions is to provide the nuclear data to the existing database related to the p process and for the validation of the statistical model codes for the broad range of nuclides.

Further, the cross sections were determined for ^{110}Cd(p, n)^{110}In & ^{110}Cd(p, 2n)^{109}In reactions for the reactor and other applications. The isotope ^{110}Cd is important for the thin layer activation analysis (TLA), medical isotope production, radioactive waste handling, etc. [1, 4, 24]. As the product nuclei ^{109,110}In have shorter half-life which is around 4.167 h and 4.92 h, respectively, these nuclei are convenient for PET studies [24]. Moreover, the scarcity of cross sections is found for ^{110}Cd(p, n)^{110}In [28, 30, 39, 40], and ^{110}Cd(p, 2n)^{109}In [28, 39] reactions. Therefore, we aim to report experimentally measured data for the ^{110}Cd(p, n)^{110}In reaction for the ground state population and ^{110}Cd(p, 2n)^{109}In reaction at 14.14 $\pm$ 2.03 MeV of energy. Also, the cross section ratio has been calculated for ^{110}Cd(p, n)^{110}In reaction as the product

nuclei ^{110}In populates to the ground state (7^+) and metastable state (2^+). The ratio of cross section is crucial for the nuclear model examination and to get a complete understanding of the mechanism behind compound nuclear reactions [41]. The ground state (σ_g) to isomeric state (σ_m) cross section ratio depends on the distribution of the compound nucleus (CN) that populated them [42] and on the spin of the states.

The activation cross sections and corresponding S factors for ^{114}Cd(p, γ)^{115m}In, and ^{114}Cd(p, n)^{114m}In, and ^{112}Cd(p, γ)^{113m}In reactions are presented in this study. The data obtained from the experiment are simulated with the theoretical data of TALYS (latest version), and with the EXFOR which is the nuclear data library of the previously published experimental data [43]. Further, the cross sections are reported for ^{110}Cd(p, n)^{110g}In, & ^{110}Cd(p, 2n)^{109}In reactions and simulated with the phenomenological and microscopic nuclear level densities (NLDs) of TALYS [44], EMPIRE [45], and ALICE [46] codes, and with the EXFOR database [43]. Only theoretical calculations were carried out for ^{110}Cd(p, n)^{110m}In, & ^{110}Cd(p, n)^{110}In reactions utilizing the above mentioned three nuclear model codes. The cross section ratio was found using theoretical models for ^{110}Cd(p, n) reaction .

This chapter is portrayed as follows: Section 5.2 includes experimental procedure. Section 5.3 is the description of the data analysis part, which explains the cross section measurement and S factor determination. The overview of theoretical calculations is included in §5.4. The obtained results are discussed in §5.5. At the end, summary and conclusions are portrayed in §5.6.

5.2 Experimental Details

The BARC-TIFR pelletron [48] facility has been utilized to deliver 16 MeV of the proton beam. The stacked foil activation method, and offline γ ray spectroscopy were utilized for the experiment. A constant current of 150 nA was used for the proton beam throughout the experiment. The natural Cadmium foils of approximately 250 microns of thickness were utilized as targets and Copper foils of 3.56 microns of thickness were used as degrader. The Copper degrader was used in between the

target foils to reduce the significant amount of proton energy. The stack used for the experiment is presented in Fig. 5.1. The proton energy degradation was estimated using SRIM code [49] as well as using Monte Carlo Simulation code MCNP-6.2 [50]. The energy degradation curve obtained using MCNP code is presented in Fig. 5.2. It is presumed that the reaction is occurring at the mid way of the target, and the effective proton energy of the experiment is considered as 14.14, 10.10, and 4.86 MeV.

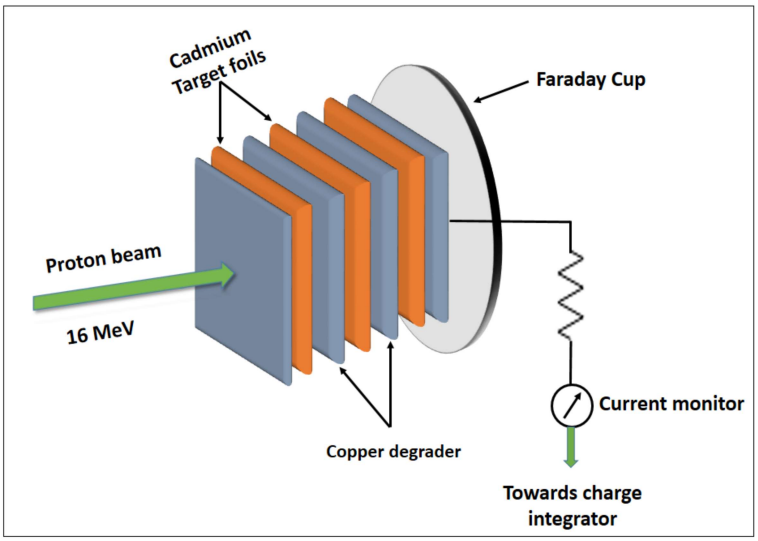

Figure 5.1: Arrangement of the stacked foil experiment [47].

For the proton irradiation, thin aluminium (Al) foil was used to wrap the stack made up of targets and degraders. This assembly was placed inside the irradiation port of 6 m for irradiation. To obtained a perfectly circular shaped proton beam, it is allowed to pass through the 6 mm aperture of a Tantalum collimator. The stack was irradiated for sufficient time to build an acceptable amount of activity. After cooling down these samples, the targets were taken for gamma ray counting. The HPGe detector was used for the counting of γ rays which was pre-calibrated with multi gamma source ^{152}Eu, and joined to 4K channel analyzer. The collected activity of targets is in the form of γ ray spectra which is presented in Fig. 5.3. The product nuclei of our interest were identified using characteristic gamma lines with their half-lives. Spectroscopic details were extracted from the NuDat database [51]. The threshold energies and Q values were extracted from QTOOL [52]. spectroscopic

details are indicated in Table 5.1.

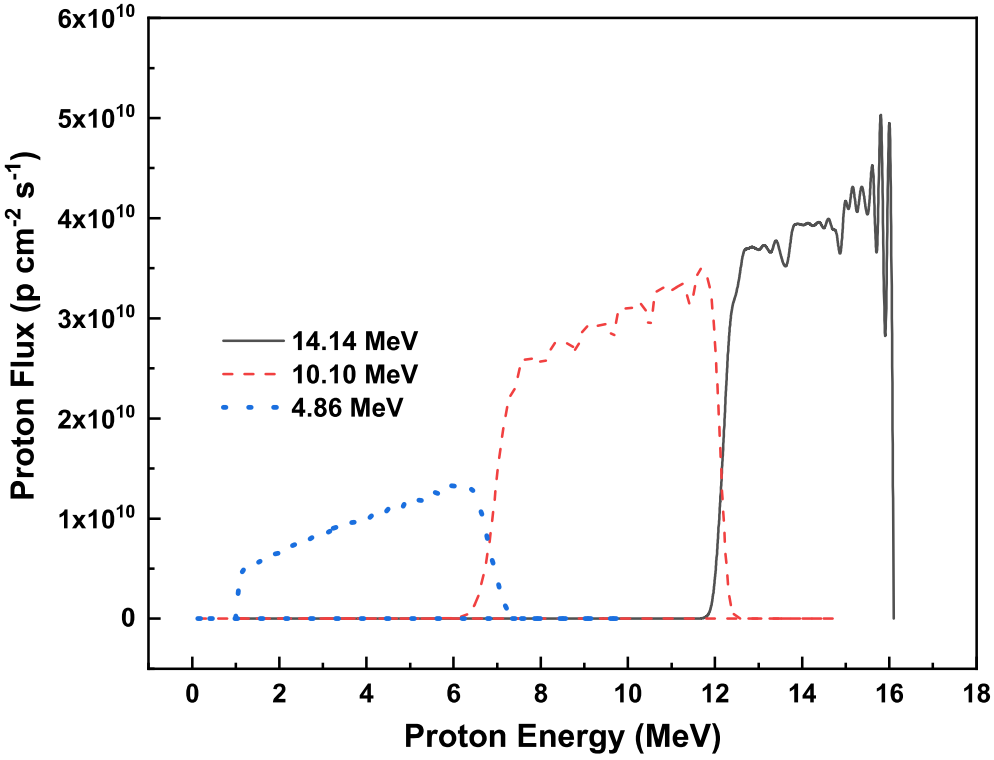

Figure 5.2: Proton energy degradation using MCNP 6.2 code. [50].

5.3 Data Analysis

5.3.1 Analyzed reactions

Natural Cadmium has eight stable nuclides with atomic mass numbers A = 106, 108, 110, 111, 112, 113, 114, and 116 having isotopic abundance 1.25 %, 0.89 %, 12.49 %, 12.80 %, 24.13 %, 12.22 %, 28.73 %, and 7.49 % [54]. The ^{114}Cd, and ^{110}Cd nuclei with their respective isotopic abundances 28.73 %, and 12.49 % have been considered for the study. Spectroscopic detail of the selected reactions are presented in Table 5.1.

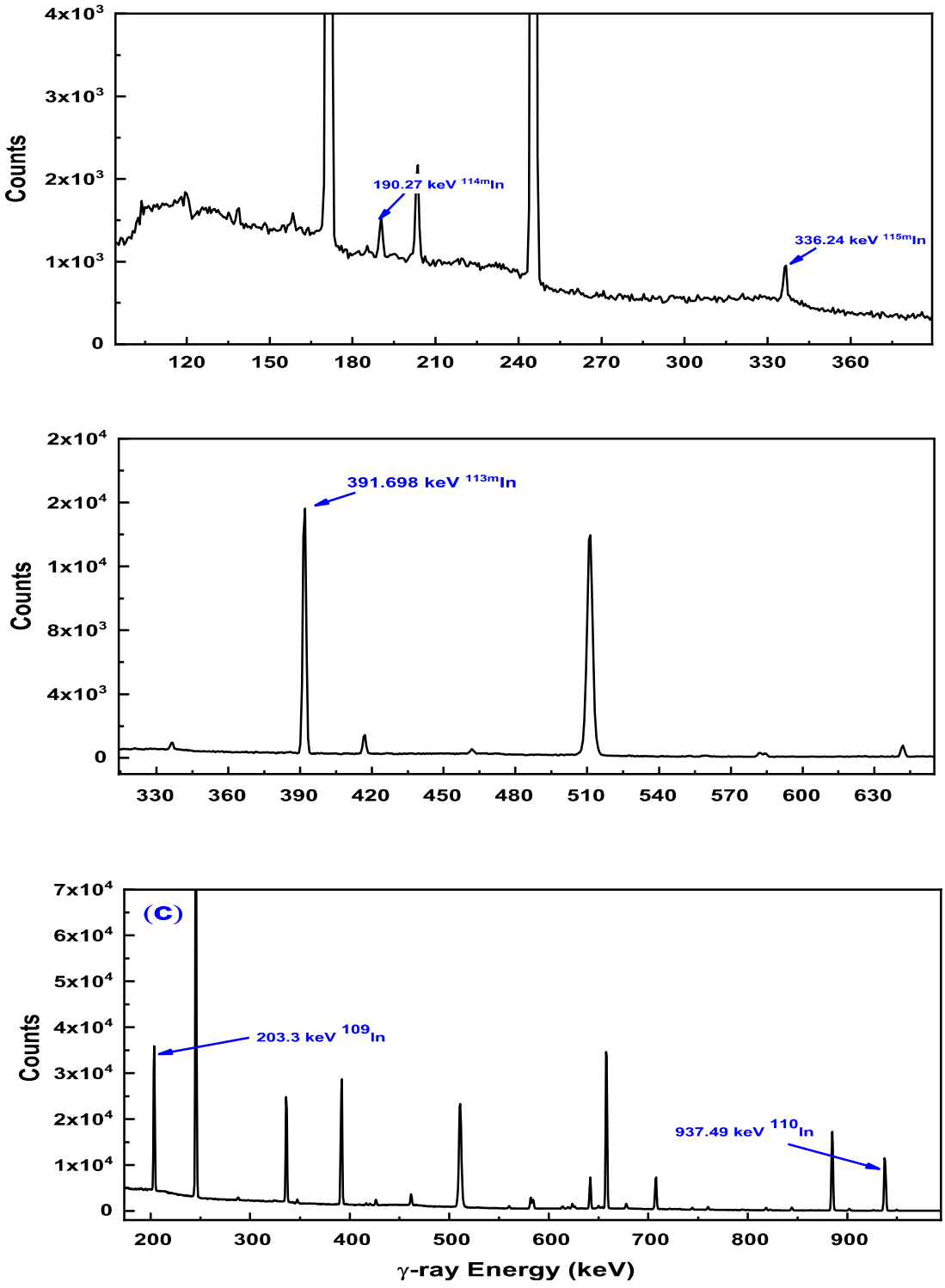

Figure 5.3: Gamma ray spectra typically obtained from the interaction of proton-Cadmium at (a) $E_p \approx 16$ MeV, (b) 7.8 MeV & (c) 16 MeV of proton energies, respectively.

Table 5.1: Isotopic abundance of samples, energy level of the resultant nuclei, threshold energy of reaction, product nucleus, spin, decay mode and half life of the product nucleus, and γ-energies with relative intensities of proffered reactions.

Reaction	E(level) (MeV)	Isotopic abundance (a) [53] (%)	Threshold energy (E_{th}) [52] (MeV)	Product nucleus	J^{π}	Decay mode	Half-life [51]	γ-ray energy (E_{γ}) [51] keV	Branching intensity (I_{γ}) (%)
^{114}Cd(p, γ)	0.3362	28.73	0.0	^{115m}In	$\frac{1}{2}^{-}$	IT : 95.00 % β^{-} : 5.00 %	4.486 (4) h	336.24 (25)	45.9 (1)
^{114}Cd(p, n)	0.1908	28.73	2.247	^{114m}In	5^{+}	IT : 96.75 % ϵ : 3.25 %	49.51 (1) d	190.27 (3)	15.56 (15)
^{112}Cd(p, γ)	0.3917	24.13	0.0	^{113m}In	$\frac{1}{2}^{-}$	IT : 100.00 %	99.476 (23)m	391.698 (3)	64.94 (17)
^{110}Cd(p, n)	0.0	12.49	4.703	^{110g}In	7^{+}	ϵ = 100.00 %	4.92 (8) h	937.478 (13) 657.75 (10)	68.4 (19) 98 (3)
^{110}Cd(p, n)	0.0621	12.49	4.703	^{110m}In	2^{+}	ϵ = 100.00 %	4.92 (8) h	657.75 (5)	97.74
^{111}Cd(p, 2n)	0.0	12.80	4.703	^{110g}In	2^{+}	ϵ = 100.00 %	4.92 (8) h	937.478 (13) 657.75 (10)	68.4 (19) 98 (3)
^{111}Cd(p, 2n)	0.0	12.80	4.703	^{110m}In	2^{+}	ϵ = 100.00 %	4.92 (8) h	657.75 (5)	97.74
^{110}Cd(p, 2n)	0.0	12.80	11.472	^{109g}In	$\frac{9}{2}^{+}$	ϵ = 100.00 %	4.159 (10) h	203.3 (1)	74.2
^{110}Cd(p, 2n)	0.6501	12.49	12.829	^{109m_1}In	$\frac{1}{2}^{-}$	IT = 100.00 %	1.34 (7) m	649.8 (2)	93.51 (9)
^{110}Cd(p, 2n)	2.1018	12.49	12.829	^{109m_2}In	$\frac{19}{2}^{+}$	IT = 100.00 %	0.209 (6) s	673.52 (8)	97.6 (3)

The ^{115}In radionuclide produced via ^{114}Cd(p, γ) reaction channel populates into the ground state and metastable state with 4.41 $\times$ 10^{14} y and 4.486 h of half-life, respectively. The measurement of cross section was performed for ^{114}Cd(p, γ)^{115m}In reaction as ^{115}In has sufficient half-life in its metastable state.

The ^{114}In radionuclide produced via ^{114}Cd(p, n) reaction channel populates into ground state with 71.9 s of half-life and two metastable states, ^{114m_1}In with half-life of 49.51 d and ^{114m_2}In with half-life 43.1 ms. The half-life of the ground state and isomeric state is shorter so that it is not feasible to measure cross section using the offline γ ray spectrometry. Therefore, the cross sections were estimated for the ^{114}Cd(p, n)^{114m_1}In reaction.

For ^{112}Cd(p, γ)^{113}In reaction, the product nuclei ^{113}In populates into ground state and metastable state. As ^{113}In is stable at its ground state whereas it's the metastable state has 1.6582 h of half-life. Therefore, the ^{112}Cd(p, γ)^{113m}In reaction has been chosen for this work.

Further, the ^{110}In and ^{109}In radionuclides are produced via (p, n), and (p, 2n) channels, respectively. The ^{109}In nuclide populates in two metastable states ^{109m_1}In with half-life $\tau_{1/2} = 1.34$ m and ^{109m_2}In with half-life $\tau_{1/2} = 0.209$ s. Due to the shorter half-life of both metastable states, after sufficient cooling time, these states decayed by 100 % IT to the ground state. Therefore, the decay of the ground state delivers the knowledge regarding production of total cross section. The ^{110}In nucleus is formed in its the ground state with spin $J^{\pi} = 7^{+}$ and populates in isomeric state with the energy $E_{level} = 62.1$ keV and $J^{\pi} = 2^{+}$ spin via ^{110}Cd(p, n) reaction channel. The cross section was measured for the ^{110}Cd(p, n)^{110g}In reaction corresponding to 937.478 keV of γ energy. The cross section measurement of metastable state population of ^{110}Cd(p, n) reaction is difficult as more than two reaction channels produce the product nuclei having the same γ energy which is 657.75 keV, and it is difficult to separate those reaction channels. Therefore, the theoretical model codes have been utilized for the prediction of cross section for ^{110}Cd(p, n)^{110m}In reaction.

5.3.2 Cross section determination

The standard activation analysis method is widely utilized for the delayed radiochemical measurement of the nuclear reactions that produced radionuclides in the same manner as in NAA technique. In the activation technique, the proton beam targeted on the target nucleus excites the nuclei and emits the characteristic γ-rays. The emitted γ-lines should have a sufficiently longer half-life & γ-branching intensity. The cross sections were calculated for the selected reactions utilizing the activation formula [55, 56] presented below:

$$\sigma_R = \frac{A_\gamma \lambda (\frac{t_c}{t_r}) e^{\lambda t_w}}{N \epsilon I_\gamma \phi (1 - e^{-\lambda t_i})(1 - e^{-\lambda t_c})} \tag{5.1}$$

The symbols have their usual meanings.

Cadmium has many isotopes so numerous reaction channels may produce the same radionuclide as a reaction product. Therefore, it is necessary to separate out the product nucleus from the merged photopeak of γ ray. We have separate out the

following reaction product from the merged photopeak of γ-ray in the present study.

- The ^{115m}In radionuclide is produced as a reaction product from ^{114}Cd(p, γ) and ^{116}Cd(p, 2n) reaction channels. ^{116}Cd(p, 2n) reaction has threshold energy of 8.099 MeV. Therefore, we have separated the activity of the photopeak for proton energies of 14.14 $\pm$ 2.03 and 10.10 $\pm$ 2.14 MeV for the estimation of cross section for ^{114}Cd(p, γ)^{115m}In reaction.

- The ^{114m}In product nucleus is produced from ^{114}Cd(p, n) and ^{113}Cd(p, γ) reaction channels. As there is no threshold energy for ^{113}Cd(p, γ) reaction channel, we have separated activity for all the three proton energies i.e., 14.14 $\pm$ 2.03, 10.10 $\pm$ 2.14 MeV, and 4.86 $\pm$ 2.40 MeV.

- The ^{110g}In radionuclide produces as a reaction product from ^{110}Cd(p, n) and ^{111}Cd(p, 2n) reactions. The ^{111}Cd(p, 2n) reaction has threshold energy of 11.472 MeV, so we have separated activity of the photopeak for proton energy of 14.14 $\pm$ 2.03 MeV for the cross section estimation of ^{110}Cd(p, n)^{110g}In reaction.

The activity of a merged photopeak has been delineated using a technique explained in the literature [57,58]. Presently, the delineation of the ^{115m}In the product nucleus is explained here as an example. The same procedure was applied for ^{114m}In and ^{110g}In product nuclei.

$$\begin{aligned} Factor &= A_{obs}from(p,\gamma)reaction/A_{obs}from(p,2n)reaction \\ &= \frac{N\sigma_{(p,\gamma)}\phi\epsilon(1-e^{-\lambda t_i})(1-e^{-\lambda t_c})e^{\lambda t_w}/\lambda}{N\sigma_{(p,2n)}\phi\epsilon(1-e^{-\lambda t_i})(1-e^{-\lambda t_c})e^{\lambda t_w}/\lambda} \\ &= \frac{a_{114}\sigma_{(p,\gamma)}}{a_{116}\sigma_{(p,2n)}} \end{aligned} \tag{5.2}$$

where a_{114} and a_{116} represent the isotopic abundances of ^{114}Cd & ^{116}Cd, respectively. σ(p, γ) and σ(p, 2n) are the calculated cross sections obtained from the TALYS for both reactions. TALYS code has been described briefly in the next section. The activity of the single reaction product was collected using the activity ratio (factor) and the total activity of the 336.24 keV γ ray of ^{115m}In from ^{114}Cd(p, γ)^{115m}In and ^{116}Cd(p, 2n)^{115m}In reactions. After separating the activity of ^{115m}In radionuclide, the individual cross sections can be measured.

5.3.3 The S factor determination

The nuclear reactions in stars will occur near the energies where the product of velocity distribution and the cross section is at maximum. The standard approximation of the Gamow window assumes that the energy dependence of the cross section σ is mainly determined by the projectile's penetration of the Coulomb barrier (the Gamow factor $e^{-2\pi\eta}$) and a part representing the weakly energy-dependent properties of the nuclear interior (the astrophysical S factor). The non-resonant reaction rate is given by [59,60],

$$< \sigma\nu >= \left(\frac{8}{\pi\mu}\right)^{\frac{1}{2}} \frac{1}{(kT)^{\frac{3}{2}}} \int_0^\infty S(E) e^{-E/kT} e^{-2\pi\eta} dE \tag{5.3}$$

where, S(E) is the astrophysical S factor defined by,

$$S(E) = \frac{\sigma(E)E}{e^{-2\pi\eta}} \tag{5.4}$$

which is assumed to be only weakly dependent on the energy E for non-resonant reactions. The astrophysical S factor is a rescaled variant of nuclear reaction's total cross-section $\sigma(E)$ which is required for many astrophysical applications specifically for the energies below the Coulomb barrier. The S factor varies much smoothly with the energy compared to the cross-section, thus allowing for safer extrapolations to the experimentally inaccessible energy range [38,61].

The second exponential in Eq. 5.3 contains the Coulomb penetration approximation through the Sommerfeld parameter η,

$$\eta = \frac{Z_1 Z_2 e^2}{\hbar} \sqrt{\frac{\mu}{2E}} \tag{5.5}$$

where, Z_1 and Z_2 describes the charges of projectile and target, respectively and μ is the reduced mass. In the Eq. 5.3, while the first exponential decreases with increasing energy, this second one increases, leading to a confined peak of the integrand, the so-called Gamow peak. The location of the peak is shifted to higher energies with respect to the maximum of the MB distribution at $E_{MB} = kT$.

The exponent can be approximated in numerical units by

$$2\pi\eta = 31.29 Z_1 Z_2 \sqrt{\frac{\mu}{E_{c.m.}}} \tag{5.6}$$

where,the reduced mass μ in [amu] (atomic mass units) and the center-of-mass energy $E_{c.m.}$ is in [keV].

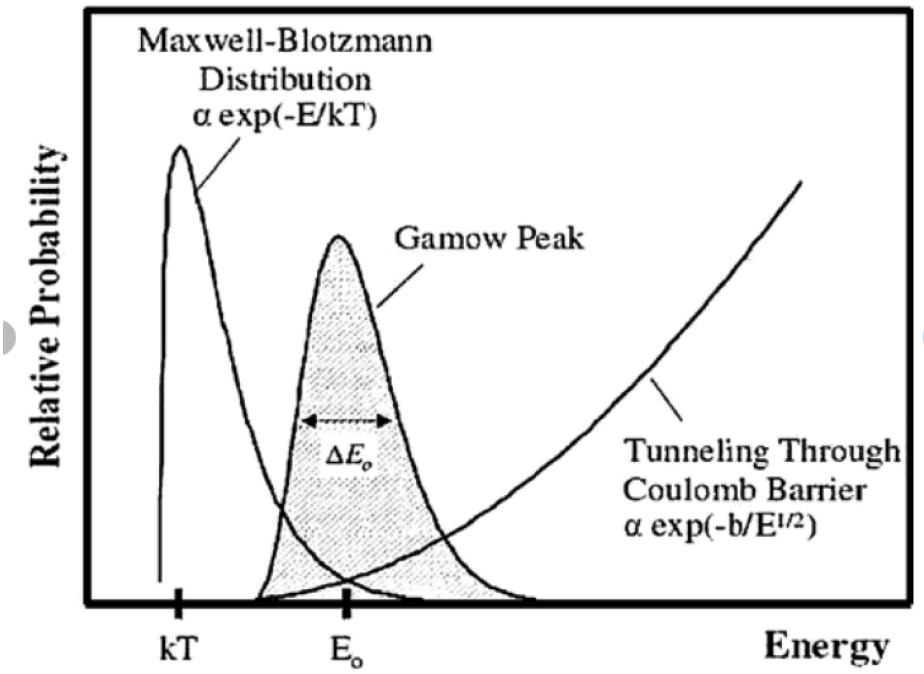

Figure 5.4: The Coulomb penetration probability folded with the Maxwell-Boltzmann velocity distribution forms the so-called Gamow peak.

The charged particle induced reactions are taking place in this relatively narrow energy window around the E_0 effective burning energy for a given stellar environment. This can be obtained by the first derivative of the integrand yields [62–64].

$$\begin{aligned} E_0 &= \left(\frac{\mu}{2}\right)^{\frac{1}{3}} (kT)^{\frac{2}{3}} \\ E_0 &= 0.12204(\mu {Z_1}^2 {Z_2}^2 {T_9}^2)^{\frac{1}{3}} \end{aligned} \tag{5.7}$$

The effective width Δ of the energy window can be define as

$$\Delta = 0.23682(\mu {Z_1}^2 {Z_2}^2 {T_9}^5)^{\frac{1}{6}} \tag{5.8}$$

Here E_0 and Δ are in units of mega-electron volts (MeV), T_9 is the plasma temperature in gigakelvins (GK), Equations 5.7 and 5.8 are widely used to determine a relevant energy range $E_0 - (\Delta/2) \leq E \leq E_0 + (\Delta/2)$ within which the nuclear cross sections have to be known. This region represents the effective energy window for non-resonant thermonuclear reactions in stars [60] which is shown in Fig. 5.4. This window shifts towards higher energy and becomes broader for increasing temperature according to Eqs. 5.7 and 5.8. These equations are important to design experiments and valid for the sufficiently low temperature and constant astrophysical S factor.

In the present study, the proton energy of 4.90±2.40 MeV lies in the range of the Gamow window for the temperatures related to the production of *p*-nuclei at T_{peak} = 5 GK. Moreover, the astrophysical S factor has been measured for ^{114}Cd(p, γ)^{115m}In, ^{114}Cd(p, n)^{114m}In, and ^{112}Cd(p, γ)^{113m}In reactions. The ^{114}Cd(p, n)^{114m}In reaction has limited utility as the reaction has [Q = - 2227.5 (0.4) keV] negative Q-value .

5.4 Theoretical Calculation

Several nuclear model codes namely, ALICE, TALYS, EMPIRE, etc. are available for the identification of reaction channels and to create nuclear data libraries. These codes predict different nuclear properties in different energy ranges using various nuclear models. We have used statistical nuclear codes such as ALICE-2014, TALYS (v. 1.95), & EMPIRE (v. 3.2.3) for the simulation of nuclear data in the present study. The aim of our theoretical study with different model codes is to acquire optimum conditions for the calculations.

5.4.1 TALYS code

The detailed description of the several reaction models has been discussed in Chapter 3. In the present study, optical models, γ- strength functions, pre-equilibrium models, and the level density (ld) models have been utilized for the cross section prediction.

The theoretical predictions were carried out using 96 different combinations of the basic constituent of the model i.e., eight γ-SFs, six NLDs, and two OMPs for ^{114}Cd(p, γ)^{115m}In, ^{114}Cd(p, n)^{114m}In, and ^{112}Cd(p, γ)^{113m}In reactions. The minimum and maximum values for each energy were defined with area of blue borders as displayed in Fig. 5.5, 5.6, & 5.7, after performing all model calculations noted in Chapter 3.

Figure 5.5 shows different combinations of TALYS code as follows: For the ^{114}Cd(p, γ)^{115m}In reaction, TALYS-1 and TALYS-2 utilize the Bauge-Delaroche-Girod OMP and the Brink-Axel (BA) Lorentzian γ-SF model, whereas TALYS-3 employs the Koning-Delaroche (KD) OMP and Kopecky-Uhl (KU) generalized Lorentzian γ-SF model; TALYS-2 and TALYS-3 include the Generalized Superfluid Model (GSM) NLD, whereas TALYS-1 employs the Back shifted Fermi gas model (BFM) NLD.

Figure 5.6 shows different combinations of TALYS code as follows: For the ^{114}Cd(p, n)^{114m}In reaction, TALYS-1 and TALYS-2 utilize the Bauge-Delaroche-Girod (JLM) OMP and TALYS -3 employs the Koning-Delaroche (KD) OMP. TALYS-1 employs HilaireâĂŹs combinatorial tables (HFB) of the NLD and Kopecky-Uhl (KU) generalized Lorentzian γ-SF model. TALYS-2 employs GorielyâĂŹs tables (HFBCS) and Hartree-Fock-Bogolyubov tables (HFB/QRPA) of the γ-SF model whereas TALYS-3 employs the generalized superfluid (GSM) NLD and T-dependent relativistic mean field (RMF) γ-SF model.

Figure 5.7 shows different combinations of TALYS code for ^{112}Cd(p, γ)^{113m}In reaction as follows: TALYS-1 employs Bauge-Delaroche-Girod OMP with Goriely's tables NLD and Brink-Axel Lorentzian γ-SF. TALYS-2 and TALYS-3 include Koning-Delaroche OMP and temperature-dependent HFB, Gogny force NLD. TALYS-2 employs Goriely T-dependent HFB γ-SF while TALYS-3 employs T-dependent RMF γ-SF.

Further, six NLD options have been utilized for the cross section estimation of ^{110}Cd(p, n)^{110g}In, ^{110}Cd(p, n)^{110m}In, ^{110}Cd(p, n)^{110}In, and ^{110}Cd(p, 2n)^{109}In reactions from threshold to 20 MeV of proton energy. We have adopted the best suitable model among them for all the reaction channels studied in the current work.

For ^{110}Cd(p, n)^{110g}In reaction, the default input parameter does not reproduce

data of the literature data, and the present measurement. Therefore, the input parameters have been modified for the reproduction of the acceptable cross sections. The adjustment in level density parameter was performed for the BFM model. The NLD formula is given in §3.2.2.1 of Chapter 3.

The asymptotic value and systematic formula of damping parameter are given below,

$$\text{asymptotic value} \quad \tilde{b} = \alpha A + \beta A^{\frac{2}{3}} \tag{5.9}$$

$$\text{damping parameter} \quad \gamma = \frac{\gamma_1}{A^{\frac{2}{3}}} + \gamma_2 \tag{5.10}$$

where, α, β, $\gamma_{1,2}$ are global parameters, and A is the atomic mass of the nuclide. The default value of a global parameter (α) is 0.0722. This value is adjusted using the keyword "alphald" to 0.1220 which is an optimum value of the BFM effective model for this reaction. The performed calculation with this adjusted parameter is plotted in Fig. 5.8-(a), and labelled as "modified BFM".

Further, the "Rspincut" keyword was used with the modified BFM to reproduce the presently measured data and previous ones. Also, this keyword is utilized to study the distribution of spin of the excited state of CN. This keyword is a multiplier to the spin cut-off parameter (σ^2). The spin cut-off parameter was multiplied by "Rspincut" keyword with the factor of 1.8 in TALYS (default value 1), to reproduce the suitable cross sections. The obtained data are plotted in Fig. 5.8-(a), and labelled as "modified BFM, Rspincut = 1.8".

5.4.2 EMPIRE code

Various nuclear models are available to study different reaction mechanisms in EMPIRE code [45]. Hauser-Feshbach formalism [65] for compound nuclear reactions, exciton model for pre-compound reaction mechanism, and optical model parameter of outgoing proton particle are taken into the consideration for this study. Out of four nuclear-level density models (three-phenomenological + One-microscopic), the best-fitted model is utilized for the study.

Moreover, to achieve a better fit with presently measured data and EXFOR data for ^{110}Cd(p, n)^{110g}In reaction, the data were obtained using the combination of the HFBM level density model with Transition Fermi densities of Monte Carlo pre-equilibrium model (FHMS) [66] and MLO3 Lorentzian ver. 3 γ strength function which is plotted in Fig. 5.8 (b).

5.4.3 ALICE code

Four different NLD options are available in the ALICE code. It is also possible to change the LD and PLD parameter of the code to obtain a considerable match of experimental measurements. The PLD can be calculated as, a PLD = A/9. The default model has been utilized for the present cross section calculation.

5.5 Results & Discussion

The activation cross sections were determined for ^{114}Cd(p, γ)^{115m}In, ^{114}Cd(p, n)^{114m}In reaction for different proton energies of 14.26 $\pm$ 2.03, 10.18 $\pm$ 2.15, and 4.90 $\pm$ 2.40 MeV in the laboratory frame, which has eminent importance for reactor applications, and the lowest energy lies in the Gamow window. The activation cross section was also estimated for ^{112}Cd(p, γ)^{113m}In reaction to the astrophysical interest for 4.90 $\pm$ 2.40 MeV in the laboratory frame. Further, The cross sections were computed for ^{110}Cd(p, n)^{110g}In and ^{110}Cd(p, 2n)^{109}In reactions at 14.14 $\pm$ 2.03 MeV of proton energy via activation method for reactor applications. The error in proton energy represents the thickness of the Cadmium target. The quadratic sum of the mentioned partial errors was considered for the estimation of uncertainty in the cross section values: counting ($\leq$ 2-3 %), efficiency of the HPGe detector ($\leq$ 3 %), mass ($\leq$ 0.001 %), and decay parameters ($\leq$ 0.5 %). Further, a theoretical study has been also accomplished for metastable and total cross sections for ^{110}Cd(p, n)^{110}In reaction using various NLDs of TALYS and EMPIRE codes, and with the default model of

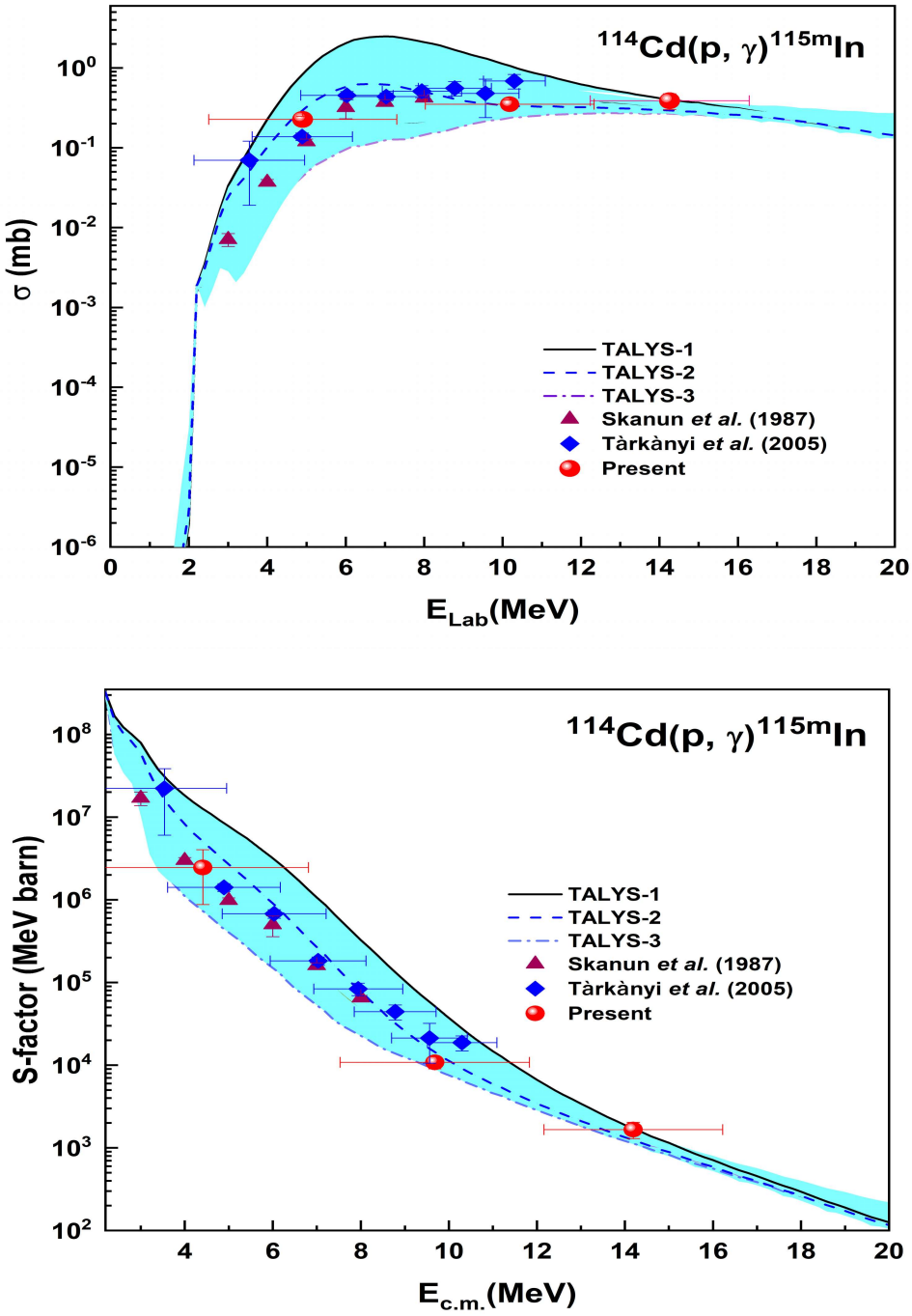

Figure 5.5: Upper panel: Comparison of the cross sections for the ^{114}Cd(p, γ)^{115m}In reaction with three different HF calculations using the TALYS-1, TALYS-2, and TALYS-3 combinations (see §5.4.1 for details) and with the data retrieved from the literature [43]. Lower panel: The corresponding astrophysical S factors.

ALICE, as it is unfeasible to measure cross sections experimentally due to shorter half-life or merging of multiple gamma rays in a photopeak.

5.5.1 ^{114}Cd(p, γ)^{115m}In reaction

The activation cross sections are simulated with the theoretical calculation of TALYS obtained with the different combinations, and the available experimental data of EXFOR [43] is presented in the upper panel of Fig. 5.5. The corresponding astrophysical S factor measured in the centre-of-mass frame is presented in the lower panel of Fig. 5.5.

The blue shaded region in the graph shows the uncertainty range of the predicted cross sections. The upper and lower borders of the shaded region associate to the highest and lowest cross section values of TALYS-1.95, respectively.

The upper border of the shaded region is the combination of JLM OMP with BSM NLD and BA γ-SF named TALYS-1. The lower border of the shaded region is the combination of KD OMP with GSM NLD and KU γ-SF named TALYS-3. The data points of 14.26 $\pm$ 2.03 and 10.18 $\pm$ 2.15 MeV lie close to the results of TALYS-2 and TALYS-3. The cross-section value of 4.90 $\pm$ 2.40 MeV is well matched with the results of TALYS-2, which is the combination of JLM OMP, GSM NLD and BA γ-SF. The presently measured data are well inside the region and has same trend of previously available data from the EXFOR data library and the predicted data of nuclear model code TALYS. The data point measured at 14.26 $\pm$ 2.03 MeV for the first time and that can help us to understand the trend. Overall the experimental data follow the trend of TALYS data and are analogous to the literature data.

5.5.2 ^{114}Cd(p, n)^{114m}In reaction

The activation cross section is compared with the theoretical calculation of TALYS obtained with the different combinations, and with the available experimental data of EXFOR [43] is presented in the upper panel of Fig. 5.6. The corresponding

astrophysical S factor measured in the centre-of-mass frame is presented in the lower panel of Fig. 5.6.

Similar to the ^{114}Cd(p, γ)^{115m}In reaction, the shaded region in the graph shows the uncertainty range of the predicted cross sections. The upper and lower borders of the shaded region related to the highest and lowest cross-section values of TALYS-1.95, respectively.

The upper border of the blue-shaded region is the combination of JLM OMP with HFB NLD and KU γ-SF named TALYS-1. The lower border of the shaded region is the combination of KD OMP with GSM NLD and T-dependent RMF γ-SF named TALYS-3. The present measurements are in the range of predicted data of TALYS. The data points of 14.26 ± 2.03 and 4.90 ± 2.40 MeV are slightly suppressed compared to the existing data points and combinations of TALYS. The cross section value of 10.18 ± 2.15 MeV is analogous to all combinations of TALYS and the literature data. The cross section value of 4.90 ± 2.40 MeV is well matched with the results of TALYS-3. Overall the experimental data follow the trend of TALYS and well matched with the literature data.

5.5.3 ^{112}Cd(p, γ)^{113m}In reaction

The measured cross section is compared with the theoretical calculation of TALYS obtained with the different combinations, and with the available experimental data of EXFOR [43] is presented in the upper panel of Fig. 5.7. The astrophysical S factor was determined using reaction cross sections and is shown in the lower panel of Fig. 5.7.

Similar to the ^{114}Cd(p, γ)^{115m}In, and ^{114}Cd(p, n)^{114m}In reactions, the shaded region in the graph shows the uncertainty range of the predicted cross sections. The upper and lower borders of the shaded region related to the highest and lowest cross-section values of TALYS-1.95, respectively.

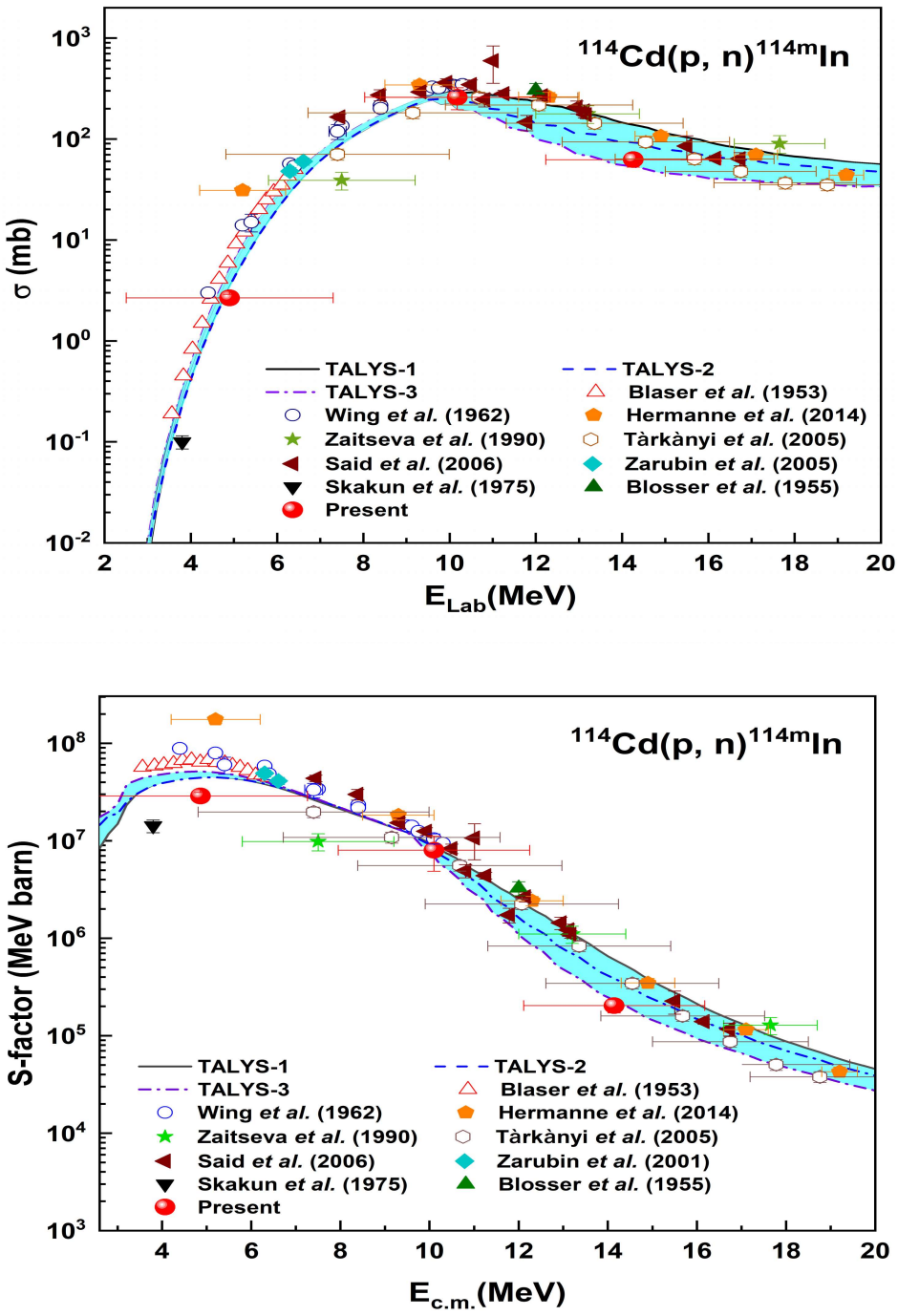

Figure 5.6: Upper panel: Comparison of the cross sections for the ^{114}Cd(p, n)^{114m}In reaction with three different HF calculations using the TALYS-1, TALYS-2, and TALYS -3 combinations (see §5.4.1 for details) and with the data retrieved from the literature [43]. Lower panel: The corresponding astrophysical S factors.

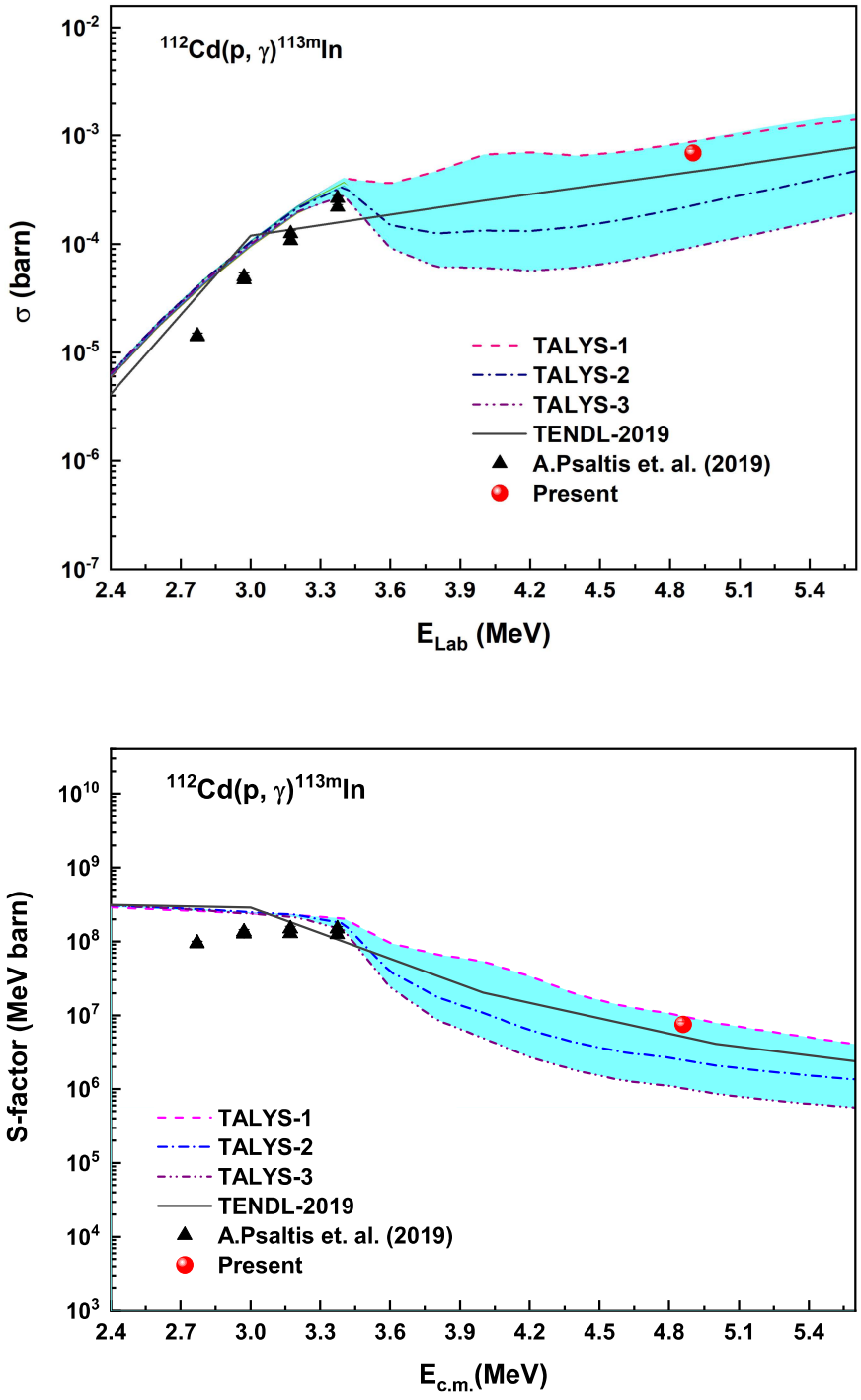

Figure 5.7: Upper panel: Comparison of the cross sections for the ^{112}Cd(p, γ)^{113m}In reaction with three different HF calculations using the TALYS-1, TALYS-2, and TALYS -3 combinations (see §5.4.1 for details) and with the data retrieved from the literature [43], and TENDL data library. Lower panel: The corresponding astrophysical S factors.

Figure 5.7 shows the measured cross section data point and also the astrophysical S factor plotted in the lower panel lie in the shaded region of TALYS-1.95 and is in good resemblance with the data of TALYS-1 and the available evaluated library TENDL-2019. The highest and lowest cross section values of TALYS are taken into account, to achieve a good description of experimental data. The measured cross-section and S factor values corresponding to 4.86 MeV of proton energy are mentioned in Table 5.2.

Table 5.2: Cross sections and astrophysical S factors for the ^{114}Cd(p, γ)^{115m}In, ^{114}Cd(p, n)^{114m}In, and ^{112}Cd(p, γ)^{113m}In reactions.

			^{114}Cd(p, γ)^{115m}In		^{114}Cd(p, n)^{114m}In		^{112}Cd(p, γ)^{113m}In	
E_p	$E_{c.m.}$	E_{lab}	Cross section	S factor	Cross section	S factor	Cross section	S factor
(MeV)	(MeV)	(MeV)	(mb)	(10^6 MeV barn)	(mb)	(10^6 MeV barn)	(mb)	(10^6 MeV barn)
16.00	14.14	14.26 ± 2.03	0.389 ± 0.087	0.0017	47.60 ± 7.53	0.2037	-	-
12.27	10.10	10.18 ± 2.15	0.351 ± 0.044	0.0108	258.72 ± 63.31	7.9908	-	-
7.83	4.86	4.90 ± 2.40	0.227 ± 0.054	2.4542	2.67 ± 0.23	28.8429	0.691 ± 0.0625	7.497

5.5.4 ^{110}Cd(p, n)^{110g}In, ^{110}Cd(p, n)^{110m}In, & ^{110} Cd(p, n)^{110}In reactions

Figure 5.8 (a) contains measured cross section value for ^{110}Cd(p, n)^{110g}In reaction compared with the data obtained from threshold energy (E_{th} = 4.703 MeV) to 20 MeV of proton energy using phenomenological NLD models of TALYS, EMPIRE and ALICE codes, and with the data retrieved data from K. Otozai *et al.* 1966 [39]. The estimated cross section value agrees well with the ESLD model of EMPIRE. The BFM model of TALYS predicts underestimated data than the other data sets. To overcome the discrepancy of the predicted data of TALYS, the calculations were modified by adjusting the relevant parameter set as mentioned in subsection §5.4.1. The obtained data after modification in parameters of TALYS (i.e, modified BFM, Rspincut=1.8) shows a better match with present measurement, predictions of the ESLD model of EMPIRE, and also with the K. Otozai *et al.* 1966 data. The predictions of ALICE

are well matched with the data of K. Otozai *et al.* 1966 at low energy range but over-predicted than the other datasets. After 16 MeV of proton energy, a slight variation is observed between model predictions. Due to the discrepancies in the predicted data of models at higher energies, it is essential to measure experimental data for validation of the codes that confirm the appropriateness of the model.

Figure 5.8 (b) shows a resemblance of presently measured experimental data with microscopic approaches of TALYS and EMPIRE predictions. Our measurement is slightly higher than the HFBM of EMPIRE-3.2.3. We have obtained theoretical data using the combination of Transition Fermi densities of the Monte Carlo pre-equilibrium model (FHMS) with HFBM level densities and MLO3-modified Lorentzian ver. 3 of γ-SF which is well matched with our data. The EXFOR data is also close to the data obtained with this combination. The predictions of TALYS are lower than the present measurement, EXFOR databases, and EMPIRE predictions.

Further, the comparison of default level density models of TALYS, EMPIRE, and ALICE along with the microscopic approaches such as TDHFB calculations using the Gogny force of TALYS, and HFBM model of EMPIRE with the previously reported data for ^{110}Cd(p, n)^{110m}In reaction is presented in Figure 5.8-(c) and for ^{110}Cd(p, n)^{110}In reaction in Figure 5.8-(d). It is observed from Figure 5.8-(c) that all the LD options are compatible with one another from the threshold to 14 MeV energy range except for ALICE data. For the higher energy, the data shows a slight discrepancy in the prediction. The previously reported data of J. -P. Blaser *et al.* (1951) [30] covers threshold energy to 6.5 MeV of energy range and is consistent with all models' predictions. Moreover, the data of K. Otozai *et al.* (1966) are also consistent with all the models except ALICE-2014. Figure 5.8-(d) depicts that all the phenomenological and microscopic approaches of TALYS and EMPIRE predictions follow the same trend for the whole range. The data are consistent for lower energy ranges but the discrepancy has been observed for higher energy ranges. The reported data of S. N. Abramovich *et al.* (1975) [40] and E. A. Skakun *et al.* (1975) [28] are lower than the theoretical predictions and hence measurement of cross section of reactions is essential to validate codes. Also, data measurement is required to enhance the data library.

The cross section ratio adversely depends on the incident energy, spins of the

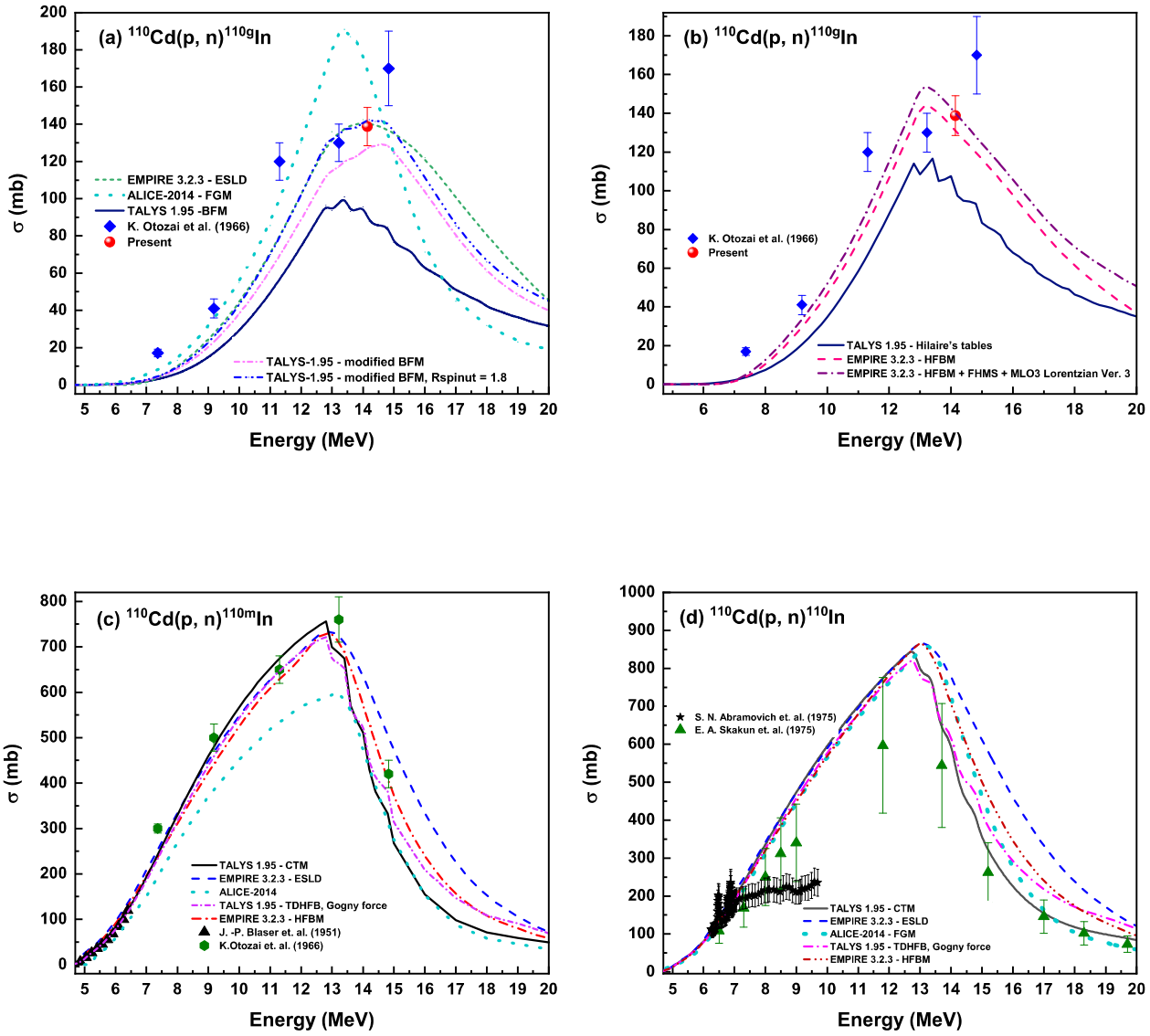

Figure 5.8: Presently measured cross section comparison of (a) ^{110}Cd(p, n)^{110g}In reaction with phenomenological models, (b) ^{110}Cd(p, n)^{110g}In reaction with microscopic models of TALYS [1], EMPIRE [17] and ALICE [38]. The theoretical predictions of (c) ^{110}Cd(p, n)^{110m}In, and (d) ^{110}Cd(p, n)^{110}In reactions using different NLDs of TALYS, EMPIRE, and default NLD option of ALICE, and with the EXFOR database [43].

ground state, and metastable state. The ratio has been calculated using theoretical model codes for ^{110}Cd(p, n) reaction from threshold (E_{th}) to 20 MeV of proton energies

and presented in Fig. 5.9 along with the ratio retrieved from EXFOR, the existing data set of E. A. Skakun *et al.* (1975) [28]. The ratio calculated using Hilaire's tables, the modified parameters of TALYS, and the GCM of EMPIRE has been plotted in Fig. 5.9. All models are well matched with the EXFOR data till 14 MeV, then the experimental data have a higher value than the predicted data.

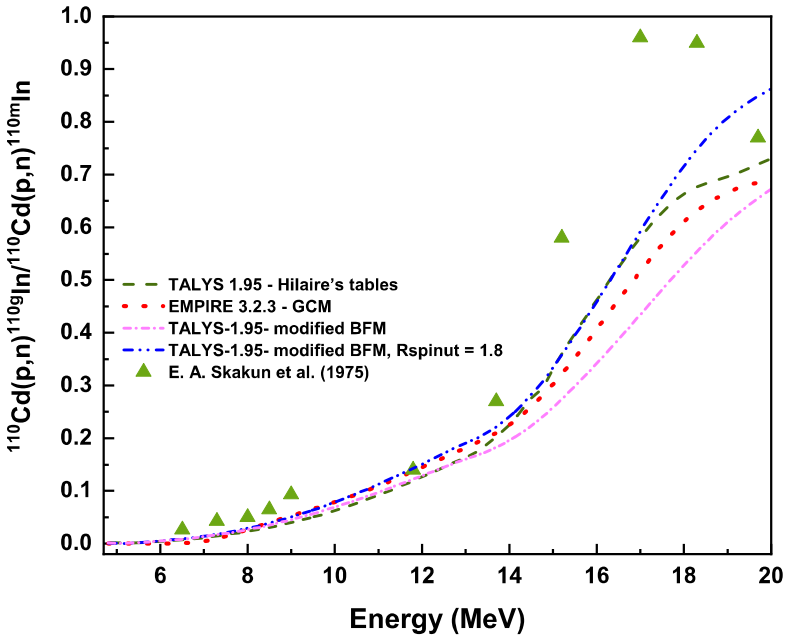

Figure 5.9: The cross section ratio of the ^{110}Cd(p, n)^{110g}In (σ_g) to ^{110}Cd(p, n)^{110m}In (σ_m) reaction for the previously measured experimental data with the theortical predictions based on the TALYS, and EMPIRE code.

In general, for the nuclei having higher spin than the metastable state, the ratio increases concerning incident energy then decreases up to some energy and remains constant for the raise in incident energy. The increasing tendency of the ratio up to a certain energy range is because of the phenomenon of compound nucleus (CN) reactions. As energy increases, the pre-compound process begins, and the ratio decreases which is due to the evaporation of the low energy nucleons occurring from the excited nucleus in the CN process. Further, the pre-compound or non-compound reaction

process initiates at higher energies in which the nucleon or nucleon clusters are emitting that remove more spin than the emission of the particle during the compound nucleus process. The large angular momentum is taken away by emitted high-energy particles during the process. Therefore, the spin distribution of the product nuclei is commonly less than the initial spin distribution [67, 68].

The ground state spin (7^+) is higher than the metastable state (2^+) of the ^{110}In nuclei, that increases the probability of the ground state population with increasing energy. Figure 5.9 also illustrates that the cross section ratio increases concerning the proton energy. This is the same behaviour observed in the compound nuclear reaction mechanism, the higher angular momentum transferred to the CN favours the formation of high-spin nuclei.

5.5.5 ^{110}Cd(p, 2n)^{109}In reaction

The cross section value evaluated with the activation method is presented in Fig. 5.10 - (a) & (b) along with theoretical predictions using different models of TALYS, EMPIRE, and default level density model of ALICE-2014 as well with the EXFOR data, MENDL-2, and TENDL-2019 evaluated data libraries.

Figure 5.10 - (a) shows the analogy of estimated data with the phenomenological model of TALYS, EMPIRE, and ALICE.

It is noticeable from the figure that experimentally measured cross section value is in the range of theoretical predictions. The earlier reported data of K. otozai *et al.* (1966) [39] also match the theoretical predictions while the data of E. A. Skakun *et al.* (1975) [28] is lower than all the level density models but nearer to the ESLD model of EMPIRE-3.2.3. As the energy increases, the discrepancy found in the data is predicted by various phenomenological models. The TENDL-2019 data and cross sections obtained using the GSM model of TALYS complement each other.

Figure 5.10 - (b) shows an analogy of presently evaluated data with the microscopic models of TALYS and EMPIRE codes. Our data falls in the range of theoretical predictions. The data obtained from Goriely's tables of TALYS-1.95 is nearer

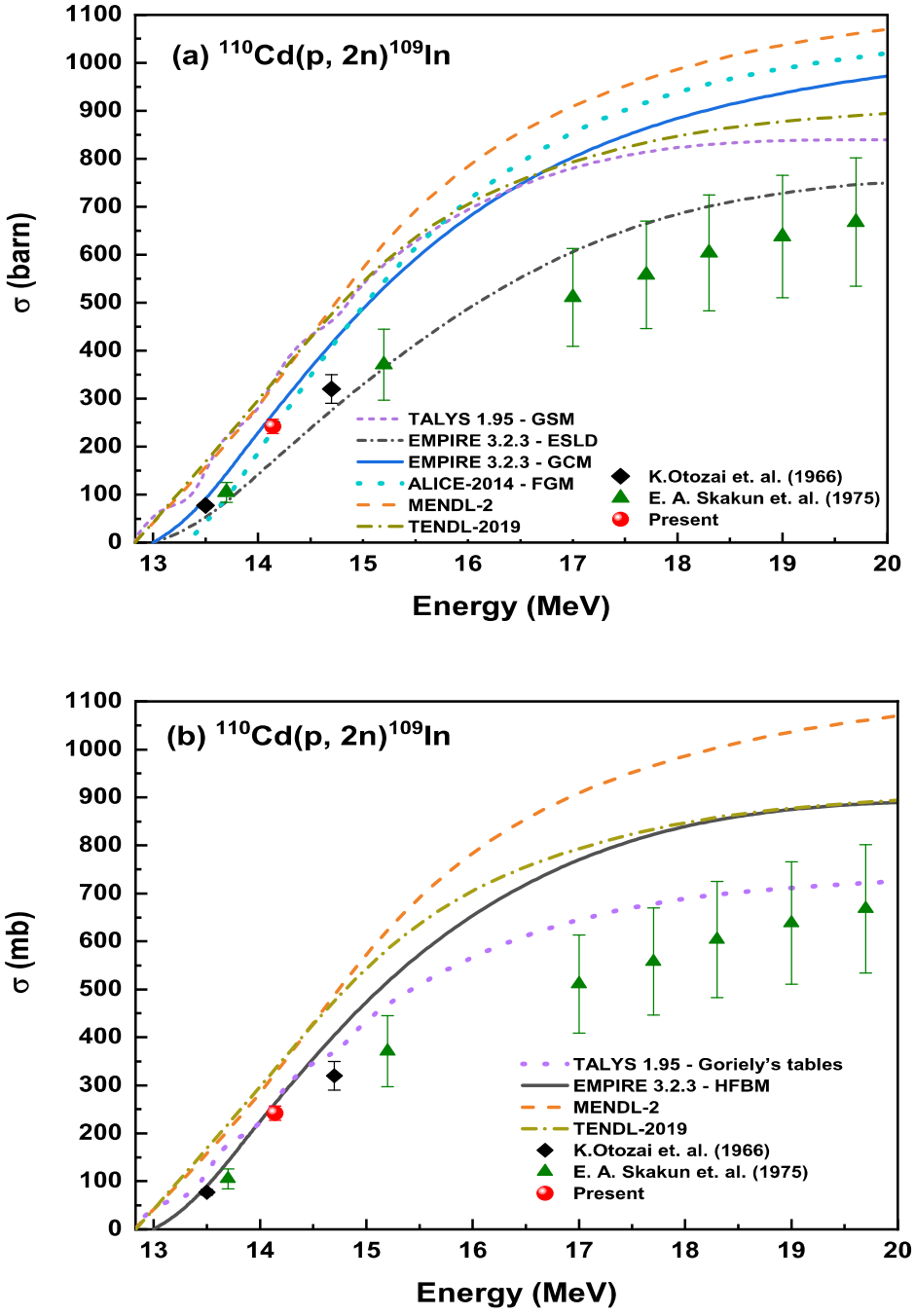

Figure 5.10: Presently measured cross section comparison of (a) ^{110}Cd(p, 2n)^{109}In reaction with phenomenological models, (b) ^{110}Cd(p, 2n)^{109}In reaction with microscopic models of TALYS, EMPIRE, ALICE and with EXFOR data. The MENDL-2 and TENDL-2019 data libraries are also included.

to the previously reported data of K. otozai *et al.* (1966) [39] & E. A. Skakun *et al.* (1975) [28] retrieved from EXFOR. The data of the TENDL-2019 library and the HFBM model of EMPIRE complement each other. The data of the MENDL-2 library is over-predicted than the data predicted using all phenomenological and microscopic approaches of presently utilized codes. At the higher energies, a discrepancy in theoretical data prediction is found. Therefore, to validate the theoretical model codes, experimental measurements are required. Moreover, the previously reported data are very old and scarce so new measurements using the latest facilities are required.

Table 5.3: Experimentally measured cross sections for ^{110}Cd(p, n) & ^{110}Cd(p, 2n) reactions.

Reactions	Energy (E_p) (MeV)	Cross section (σ) (mb)
^{110}Cd(p, n)^{110g}In	14.14 ± 2.03	139 ± 10
^{110}Cd(p, n)^{109}In	14.14 ± 2.03	242 ± 15

5.6 Summary and Conclusion

Multidisciplinary work has been accomplished in the nuclear reactors and astrophysics. This work was performed to enhance the nuclear data library of proton induced nuclear reactions as well as a contribution to the p process reaction network. The irradiation experiment on Cadmium was carried out utilizing the stacked foil activation analysis method and offline γ ray spectrometry.

The cross sections were determined for ^{114}Cd(p, γ)^{115m}In, ^{114}Cd(p, n)^{114m}In reactions for three different proton energies, 14.26 ± 2.03, 10.18 ± 2.15, and 4.90 ± 2.40 MeV, while the cross section of ^{112}Cd(p, γ)^{113m}In reaction was evaluated at 4.90± 2.40 MeV of energy in the laboratory frame. The cross sections were simulated with the previously reported literature data and the data obtained from the combination of nuclear models of the TALYS code. The astrophysical S factor was also determined for all three reactions in the centre of mass frame.

The cross sections were evaluated for ^{110}Cd(p, n)^{110g}In and ^{110}Cd(p, 2n)^{109}In reactions at 14.14 ± 2.03 MeV of proton energy, and compared with the EXFOR data, the theoretical prediction obtained using phenomenological and microscopic approach of TALYS, and EMPIRE code, and with the default level density of ALICE code.

The phenomenological BFM model of TALYS was modified with the level density and spin-cut-off parameter which shows good resemblance with presently measured data, EMPIRE data, and with previously reported data of EXFOR for ^{110}Cd(p, n)^{110g}In reaction. Further, to achieve resemblance in the microscopic approach, the combination of HFBM + FHMS + MLO3 modified Lorentzian ver. 3 of γ-SF of EMPIRE was adopted which shows fairly good agreement with presently measured data and EXFOR data. However, Predictions of TALYS are underestimated for the reaction. The isomeric state population of ^{110}Cd(p, n)^{110}In reaction and total cross sections were studied using TALYS, EMPIRE, and ALICE codes, and comparison with previously reported data shows good agreement. Further, the data produced using a default model of ALICE-2014 code are under/over-predicted for the reaction. The cross section ratio (σ_g/σ_m) has been also studied theoretically for the ^{110}Cd(p, n) reaction that shows the CN mechanism. The experimentally measured cross section of ^{110}Cd(p, 2n)^{109}In reaction also shows good resemblance with theoretical predictions of TALYS, EMPIRE, and ALICE. However, the data libraries MENLDL-2 and TENDL-2019 are over-predicted.

Overall, the present study observes that less experimental data are available for the chosen reactions. Therefore, experimental measurements are required for theoretical code validation and the advancement and improvement of nuclear reactors and medical accelerators, the accurate measurement of reaction data is very important. Also, it is important to study theoretical and experimental aspects to achieve a deep understanding of the driving mechanism behind the astrophysical p process.

Bibliography

[1] F. Tàrkànyi *et al.*, Nucl. Instrum. Methods Phys. Res., Sect. B **245**, 379-394 (2006).

[2] E. Alhassan *et al.*, EPJ Web Conf. **239**, 13005 (2020).

[3] Mayeen Uddin Khandaker *et al.*, Nucl. Instr. and Meth. in Phys. Res. B **333**, 80-91 (2014).

[4] M. Al-Abyad, J. Rad. Res. Appl. Sci., Vol. **5**, No. 2 (2012).

[5] F. Carminati *et al.*, An Energy Amplifier for Cleaner and Inexhaustible Nuclear Energy Production Driven by Particle Beam Accelerator, CERN Report No. CERN/AT/93-47 (ET), 1993 (unpublished).

[6] C. Rubbia *et al.*, Conceptual Design of a Fast Neutron Operated High Power Energy Amplifier, CERN Report No. CERN/AT/95-44 (ET), 1995 (unpublished).

[7] The International Conference on Accelerator-Driven Transmutation Technologies and Applications, Las Vegas, Nevada, 1994, edited by E. D. Arthur, S. A. Schriber, and A. Rodriguez, AIP Conf. Proc. No. **346** (AIP, New Yotk, 1995).

[8] Muhammad Shahid *et al.*, Nucl. Instrum. Methods Phys. Res. Sect. B **342**, 305 (2015).

[9] R. K. Sinha and A. Kakodkar, Nucl. Eng. Des. **236**, 683 (2006).

[10] S. Ganesan, Creation of Indian Experimental Benchmarks for Thorium Fuel Cycle, IAEA Coordinated Research Project on Evaluated Data for Thorium-Uranium fuel Cycle, Third Research Co-ordination Meeting, 30 January to 2 February 2006, Vienna, Austria, IAEA Report No. INDC(NDS)-0494, 2006 (unpublished).

[11] F. -R. Lecolley *et al.*, in International Conference on Nuclear Data for Science and Technology, 26 September - 1 October 2004, Santa Fe, edited by R. C. Haight, M. B. Chadwick, T. Kawano, and P. Talou, AIP Conf. Proc. No. **769** (AIP, New York, 2005), p. 61.

[12] G. R. Grant and L. Yaffe, Can. J. Chem. **41**, 2533 (1963).

[13] T. Allen *et al.*, Mater. Today **13**, 14 (2010).

[14] S. S. Glickstein and R. G. Winter, Nucl. Instrum. Methods **9**, 226 (1960).

[15] E. M. Burbidge, G. R. Burbidge, W. A. Fowler, and F. Hoyle, Rev. Mod. Phys. **29**, 547 (1957).

[16] A. G. W. Cameron, Publ. Astron. Soc. Pac. **69**, 201 (1957).

[17] M. Arnould and S. Goriely, Phys. Rep. **384**, 1 (2003).

[18] C. Travaglio *et al.*, Astrophys. J. **739**, 93 (2011).

[19] F. A. Cotton and G. Wilkinson, Zinc, cadmium and mercury, Advanced inorganic chemistry. 3^{rd} edition. Inter science Publishers. p. 503 (1972).

[20] D. A. Petti, Nucl. Technol. **84**, 128 (1989).

[21] K. A. Mahmoud *et al.*, Ceramics International, Vol. **46**, Issue 15, 23337-23346 (2020).

[22] S. T. Mongelli *et al.*, Braz. J. Phys. **35**, 894 (2005).

[23] Y. S. Alajerami *et al.*, J. Appl. Phys. **127**, 175102 (2020).

[24] F. S. Al-Saleh, Radiochim. Acta **96**, 461 (2008).

[25] F. Ditrói *et al.*, Appl. Radiat. Isot. **118**, 266-276 (2016).

[26] Camilo Rios and Marisela Mèndez-Armenta, Encyclopedia of Environmental Health, 2^{nd} Edition, 485-491 (2019).

[27] B. M. Ali *et al.*, Nucl. Instr. and Meth. in Phys. Res. B **321**, 30-40, (2014).

[28] E. A. Skakun *et al.*, Yad. Fiz. **45**, 614 (1987).

[29] F. Tàrkànyi *et al.*, Radiochim. Acta **93**, 561 (2005).

[30] J. -P. Blaser *et al.*, Helv. Phys. Acta **24**, 3 (1951).

[31] J. Wing and J. R. Huizenga, Phys. Rev. **128**, 280 (1962).

[32] A. Hermanne *et al.*, Radiochimica Acta. **102**, 1111 (2014).

[33] N. G. Zaitseva *et al.*, Appl. Radiat. Isot. **41**, 177 (1990).

[34] S. A. Said, E. K. Elmaghraby, and F. I. Asfour, Appl. Radiat. Isot. **64**, 1655 (2006).

[35] P. P. Zarubin and V. O. Sergeev, Ross. Akad. Nauk, Ser. Fiz. **65**, 1612 (2001).

[36] E. A. Skakun *et al.* Izvestiya Ross. Akad. Nauk, Ser. Fiz. **39**, 24 (1975).

[37] H. G. Blosser and T. H. Handley, Phys. Rev. **100**, 1340 (1955).

[38] A. Psaltis *et. al.*, Phy. Rev. C **99**, 065807 (2019).

[39] K. Otozai *et al.*, Nuclear Physics **80**, 335-348 (1966).

[40] S. N. Abramovich *et al.*, Izv. Rossiiskoi Akademii Nauk, Ser.Fiz., Vol. **39**, p. 1688 (1975).

[41] N. Patronis *et al.*, Phys. Rev. C **75**, 034607 (2007).

[42] E. Georgali *et al.*, Phys. Rev. C **102**, 034610 (2020).

[43] Cross-Section Information Storage and Retrieval System (EXFOR), IAEA, Vienna, `http://www.nds.iaea.or.at/exfor/`.

[44] A. J. Koning, S. Hilaire, and S. Goriely, TALYS user manual, A nuclear reaction program, NRG-1755 ZG PETTEN, The Netherlands, (2017).

[45] M. Herman *et al.*, "EMPIRE (ver. 3.2.3): Nuclear Reaction Model Code System for Data Evaluation", Users Manual, INDC(NDS)-0603 (2015).

[46] M. Blann, Phys. Rev. Lett. **27**, 337 (1971).

[47] S. Parashari *et al.*, Nucl. Phys. A **979**, 102 (2018).

[48] BARC-TIFR Pelletron facility, Mumbai, official website: `https://www.tifr.res.in/~pell/pelletron/`.

[49] James F. Ziegler, M. D. Ziegler, and J. P. Biersack, Nucl. Instrum. and Meth. in Phys. Res. B **268**, 1818-1823 (2010).

[50] C. J. Werner (editor), "MCNP Users Manual - Code Version 6.2", Los Alamos National Laboratory, report LA-UR-17-29981 (2017).

[51] NuDat 2.7β2011, National Nuclear Data Center, Brookhaven National Laboratory, official website: `https://www.nndc.bnl.gov/nudat2/`

[52] Qtool: calculation of reaction Q-values and threshold, Los Alamos National Library, official website: `http://cdfe.sinp.msu.ru/services/calc_thr/calc_thr.html`

[53] K. J. R. Rosman, and P. D. P. Taylor, Pure Appl. Chem. **70**, 217 (1998).

[54] Chart of Nuclides, National Nuclear Data Center, Brookhaven National Laboratory, Official webpage: `https://www.nndc.bnl.gov/chart/`

[55] R. Makwana *et al.*, Phys. Rev. C **96**, 024608 (2017).

[56] V. Vashi *et al.*, Eur. Phys. J. Plus **136**, 746 (2021).

[57] D. L. Smith *et al.*, Nucl. Phys. A **388**, 37 (1982).

[58] Reetuparna Ghosh *et al.*, J Radioanal Nucl. Chem. **307**, 1481 (2016).

[59] Thomas Rauscher, Friedrich-Karl Thielemann, and Karl-Ludwig Kratz, Phys. Rev. C **56**, Number 3 (1997).

[60] J. R. Newton *et al.*, Phys. Rev. C **75**, 045801 (2007).

[61] Vinay Singh, Joydev Lahiri, and D. N. Basu, Nucl. Phys. A **987**, 260-273 (2019).

[62] C. E. Rolfs and W. S. Rodney, Cauldrons in the Cosmos University of Chicago Press, Chicago, (1988).

[63] W. A. Fowler, G. E. Caughlan, and B. A. Zimmerman, Anu. Rev. Astron. Astrophys. **5**, 525 (1667).

[64] Thomas Rauscher, Phys. Rev. C **81**, 045807 (2010).

[65] W. Hauser and H. Feshbach, Phys. Rev. **87**, 366 (1952).

[66] M. Blann, Phys. Rev. C **54**, 1341 (1996).

[67] B. Sateesh and M. M. Musthafa, Internat. J. Modern Phys. E **21**, 1250059 (2012).

[68] K. Kim *et al.*, Nucl. Phys. A **935**, 65-78 (2015).